Author Manuscript

Author Manuscript

Author Manuscript

Author Manuscript

HHS Public Access

Author manuscript

Cancer Res. Author manuscript; available in PMC 2020 April 15.

Published in final edited form as:

Cancer Res. 2019 October 15; 79(20): 5394–5406. doi:10.1158/0008-5472.CAN-19-0381.

Nanoparticle encapsulation of synergistic immune agonists enables systemic co-delivery to tumor sites and interferon β-driven anti-tumor immunity

Prabhani U. Atukorale[1,2], **Shruti P. Raghunathan**[†,1], **Vanitha Raguveer**[†,1], **Taylor J. Moon**[1], **Carolyn Zheng**[1], **Peter A. Bielecki**[1], **Michelle L. Wiese**[1], **Amy L. Goldberg**[1], **Gil Covarrubias**[1], **Christopher J. Hoimes**[2], **Efstathios Karathanasis**[1,2,3,4,*]

[1]Department of Biomedical Engineering, Case Western Reserve University, Cleveland OH

[2]Case Comprehensive Cancer Center, Case Western Reserve University, Cleveland OH

[3]Department of Radiology, Case Western Reserve University, Cleveland OH

[4]Case Center for Imaging Research, Case Western Reserve University, Cleveland OH

Abstract

Effective cancer immunotherapy depends on the robust activation of tumor-specific antigen-presenting cells (APCs). Immune agonists encapsulated within nanoparticles can be delivered to tumor sites to generate powerful anti-tumor immune responses with minimal off-target dissemination. Systemic delivery enables widespread access to the microvasculature and draining to the APC-rich perivasculature. We developed an immuno-nanoparticle co-loaded with cyclic diguanylate monophosphate (cdGMP), an agonist of the Stimulator of Interferon Genes (STING) pathway, and monophosphoryl lipid A (MPLA), a Toll-like receptor 4 (TLR4) agonist, which synergize to produce high levels of Type I interferon β. Using a murine model of metastatic triple-negative breast cancer, systemic delivery of these immuno-nanoparticles resulted in significant therapeutic outcomes due to extensive upregulation of APCs and natural killer (NK) cells in the blood and tumor compared to control treatments. These results indicate that nanoparticles can facilitate systemic delivery of multiple immune-potentiating cargoes for effective APC-driven local and systemic anti-tumor immunity.

Keywords

cancer immunotherapy; nanoparticles; systemic delivery; triple-negative breast cancer; metastasis; STING-TLR4 synergy; interferon β

[*]Corresponding author: Efstathios Karathanasis, 1900 Euclid Avenue, Wickenden Building, Cleveland, Ohio 44106, USA, phone: 216-368-4617; stathis@case.edu.
[†]These authors contributed equally.

Conflict of interest statement
There are no conflicts to declare.

Data and Material Availability Statement
All data generated and analyzed in this study are included in this article (and its supplementary data files).

Author Manuscript Author Manuscript Author Manuscript Author Manuscript

INTRODUCTION

Generation of effective tumor site-specific immunity is pivotal to the success of an immunotherapy and depends on the robust activation of local antigen-presenting cells (APCs), such as dendritic cells (DCs) and macrophages (1–3). Immunostimulatory small molecules, cytokines, and antibodies delivered to the tumor site can generate powerful local anti-tumor immune responses individually or in specific synergistic combination (4–7). Systemic delivery enables ready access to the APC-rich perivascular areas of the tumor and has significant advantages over local delivery. Local administration depends on accurate prior knowledge of tumor sites, which is often clinically infeasible, and has limitations in the spreading of therapeutics throughout the tumor microvasculature (8–10). Systemic delivery further enables access to sites of metastasis, which are nearly impossible to clinically detect and treat early and therefore a significant contributor to mortality (11). The challenges to systemic delivery, however, are minimizing off-target toxicity and, in the case of delivering multiple synergistic therapeutics, guaranteeing co-delivery to the same target cells (12,13). Towards this goal, we present a nanotechnology approach to ‘re-engineer’ tumor site-specific immunity by co-encapsulating two synergistic immune-potentiating agents within a single liposomal nanoparticle that is delivered systemically to accumulate preferentially within the APC-rich perivascular areas of the tumor and drive an IFNβ-mediated anti-tumor immune response. Co-encapsulation within a nanoparticle not only prevents toxic systemic dissemination of these therapeutics, but also guarantees their co-delivery to the same target cell (3,14). We selected the 4T1 murine model of triple-negative breast cancer (TNBC) as an optimal test-bed for this therapy since it is poorly immunogenic with spontaneous metastasis and profound immunosuppression, as is reminiscent of clinical TNBC (15–17). A total of 12–17% of newly diagnosed early breast cancers are TNBCs, which form the most aggressive subset of breast cancer with a very high risk of recurrence and metastasis, leading to disproportionate mortality (15,18–24). Our strategy to drive local tumor site-specific immunity can have significant impact on treatment, which is otherwise severely limited.

Effective activation of local APCs plays a central role in anti-tumor immunity since these cells bridge the innate and adaptive arms of the immune system. Activated APCs help recruit and activate T and B cells that mediate tumor clearance and generate immunological memory (1,25). APC activation requires both the internalization of tumor antigens, which are readily available within the tumor microenvironment (TME) itself, as well as a strong immune-potentiating stimulus. As such, our goal was to systemically deliver a robust immune-potentiating stimulus *via* a tumor-draining nanoparticle that is readily available and amenable for uptake by APCs. Nanoparticles delivered systemically have been shown to be highly uptaken by perivascular macrophages in tumor sites and remain collected within these cells for prolonged periods of time (26). We hypothesized that harnessing multiple overlapping innate immune pathways could trigger a more potent, synergistic cytokine response. We elected to co-deliver two strong inducers of Type I interferons: Stimulator of Interferon Genes (STING) agonist cyclic diguanylate monophosphate (cdGMP) (27), which has gained significant attention in recent years, and Toll-like receptor 4 (TLR4) agonist monophosphoryl lipid A (MPLA) (28), which was clinically approved for use as the first molecular vaccine adjuvant in humans. Both cdGMP and MPLA are widely used as vaccine

Author Manuscript Author Manuscript Author Manuscript Author Manuscript

adjuvants and target host pattern recognition receptors (PRRs), which recognize conserved, immunogenic molecules from viruses and bacteria (*i.e.*, specific nucleic acids, cell membrane components) to trigger the appropriate immune response. STING agonists are cyclic dinucleotides and small-molecule second messengers that, when free in the cytosol, bind STING machinery to trigger the robust production of Type I interferons (27,29–32). The engagement of STING machinery has also been shown to activate natural killer (NK) cells that can directly attack tumor cells (2,33). MPLA is sensed by transmembrane TLR4 and has been shown to trigger a strong pro-inflammatory Th1 cytokine response (28,34). Studies have shown that direct intratumoral injection of nanoparticles loaded with STING agonists resulted in sufficient therapeutic efficacy in the B16F10 melanoma model in mice (33,35). Further, nanoparticles loaded with STING agonists or MPLA have shown promise as vaccine adjuvants that drain to lymph nodes (36).

Specifically, we exploited the leaky endothelium (37,38) of advanced TNBC tumors to achieve efficient draining of systemically delivered ~60-nm cdGMP/MPLA-encapsulated immuno-nanoparticles (immuno-NPs, Fig. 1). For our primary investigations, we selected the 4T1 murine model of metastatic TNBC as a clinically relevant test model, where orthotopic inoculation of cells in the mammary fat pad has been shown to lead to metastasis predominantly in the lungs and lymph nodes (Fig. 1a) (17). To illustrate the broad application of immuno-NPs, we selected an all-purpose, versatile liposome and co-encapsulated both hydrophilic cdGMP (within the core) and hydrophobic MPLA (within the lipid bilayer) on the same nanoparticle (Fig 1b). We elected to use relatively smaller liposomes in the 60-nm size range because of their established benefits in draining to and retention within tumors (8,37,38) and we incorporated a poly(ethylene glycol) (PEG) coating for improved solubility and circulation. The systemic administration of our immuno-NPs resulted in significant intratumoral deposition in both the primary tumor and sites of metastasis, predominantly in APC-rich perivascular regions of the TME. Upon internalization of the nanoparticles, released cdGMP and MPLA triggered a robust, synergistic site-specific cytokine gradient driven largely by IFNβ that resulted in APC- and NK cell-driven local and systemic immune recruitment (Fig. 1c).

MATERIALS AND METHODS

Nanoparticle synthesis & characterization

To synthesize nanoparticles, lipid films were prepared consisting of 48.5 mol% DOPC (1,2-dioleoyl-*sn*-glycero-3-phosphocholine, Avanti), 48.5 mol% DPPC (1,2-dipalmitoyl-*sn*-glycero-3-phosphocholine, Avanti, Alabaster, AL), and 3 mol% mPEG2000-DSPE (methoxy-poly(ethylene glycol)-2000 1,2-distearoyl-*sn*-glycero-3-phosphoethanolamine-N, Laysan Bio, Arab, AL). MPLA (100 μg per 42 μmol lipid) was added prior to film formation (Sigma-Aldrich, St. Louis, MO). Lipid films were hydrated in phosphate-buffered saline (PBS) containing 200 μg cyclic di-GMP (InvivoGen, San Diego, CA), heated to 60°C for 1 hr, and vortexed for 30 sec every 10 min. Samples were ultra-sonicated on ice for 5 min at alternating power settings (7W and 5W every 30 sec). Nanoparticles were dialyzed in PBS for 2–4 hr and stored at 4°C. Size and surface charge were measured *via* DLS and zeta potential measurements, respectively (Beckman Coulter, Brea, CA). Encapsulated cyclic di-

Author Manuscript Author Manuscript Author Manuscript Author Manuscript

GMP was measured using size exclusion HPLC (high permeation liquid chromatography, Shimadzu, Kyoto, Japan). Stability studies were conducted at 25°C and 37°C. For immuno-NP fluorescence studies, NPs were synthesized by incorporating 0.2 mol% of DiI, DiD, or DiR purchased from Thermo Fisher Scientific (Waltham, MA).

IACUC Statement

All animal studies were carried out following institutional, local, state, and federal guidelines under an IACUC-approved protocol.

Cell lines & animal models

Murine B16F10 melanoma cells and RAW 264.7 macrophages (ATCC, Manassas, VA) were cultured in DMEM medium (Gibco, Gaithersburg, MD) containing 10% fetal bovine serum (FBS, HyClone, Logan, UT). Murine 4T1 triple-negative breast cancer cells expressing green fluorescent protein (GFP) and luciferase (a gift from the Schiemann Laboratory at the Case Comprehensive Cancer Center, Cleveland, OH) were cultured in RPMI medium (Gibco, Gaithersburg, MD) containing 10% FBS. STR authentication was used for cell line authenticity. Cell lines were routinely tested and confirmed to be free of Mycoplasma contamination.

For 4T1 studies, BALB/c mice (Jackson Laboratories, Bar Harbor, ME) were inoculated by orthotopic injection of 5×10^5 4T1 cells in mammary fat pad #9. Tumors were monitored by bioluminescence imaging (BLI, IVIS Spectrum, Perkin Elmer, Waltham, MA) and caliper measurements. Tumor-bearing animals were treated on day 10 after inoculation. Nanoparticles and free immuno-agents were administered by intravenous (i.v.) or intratumoral (i.t.) injection as noted. Anti-PD-1 (250 μg, clone RMP1–14) and anti-CTLA-4 (100 μg, clone 9D9) (BioXCell, West Lebanon, NH) were administered by intraperitoneal (i.p.) injection. For ALT/AST measurements of hepatotoxicity, mice were bled retro-orbitally and serum was analyzed by the University Hospitals Pathology Core (Cleveland, OH).

For B16F10 studies, C57/BL6 mice (Jackson Laboratories, Bar Harbor, ME) were inoculated by orthotopic subcutaneous (s.c.) injection of 1×10^6 B16F10 cells on the dorsal flank. Tumors were monitored by caliper measurements. Tumor-bearing animals were treated on day 7 after inoculation. Nanoparticles were administered by i.v. injection.

Spectrum fluorescence imaging

For Spectrum studies, fluorescent nanoparticles were prepared with 0.2 mol% DiD (Invitrogen, Carlsbad, CA). 4T1 tumor-bearing mice were injected with fluorescent nanoparticles and either live-animal imaging or imaging of whole excised organs was performed using an IVIS Spectrum. Quantitative biodistribution of nanoparticles in the blood plasma was calculated using a value of 77 mL/kg for average total blood volume of a mouse (Jackson Laboratories, Bar Harbor, ME).

Author Manuscript Author Manuscript Author Manuscript Author Manuscript

Fluorescence molecular tomography

For fluorescence molecular tomography (FMT) studies, fluorescent nanoparticles were prepared with 1 mol% DSPE-VivoTag-800 (Perkin Elmer, Waltham, MA). 4T1 tumor-bearing mice were injected with fluorescent nanoparticles, euthanized at noted time points, and FMT (Perkin Elmer, Waltham, MA) was used to image whole excised organs.

Flow cytometry

Anti-mouse CD45 (30-F11), Ly-6G (1A8), Ly-6C (AL-21), CD11b (M1/70), CD11c (HL3), F4/80 (BM8), CD49b (DX5), CD3ε (145–2C11), CD4 (GK1.5), CD8α (Ly-2, 53–6.7), and CD19 (1D3) flow cytometry antibodies were purchased from BD Biosciences (San Jose, CA). Flow cytometry analysis was performed 48 hr after treatment. Blood samples were obtained *via* retro-orbital bleeding and mice were euthanized immediately afterwards and tumors and spleens were harvested. Organs were gently disrupted into single-cell suspensions in progressive steps. Cells were stained to identify immune cell populations with a blocking step using anti-mouse CD18/CD32 and analyzed using a BD FACS LSR II flow cytometer (Becton Dickinson, Franklin Lakes, NJ). FlowJo software was used to analyze data. For intracellular IFNβ staining, surface-stained cells were fixed and permeabilized (Fix/Perm Wash Buffer, BioLegend, San Diego, CA), stained with anti-IFNβ (Abcam, Cambridge, MA), and followed by secondary antibody staining.

ELISA

Six million RAW 264.7 cells were plated in triplicate per well of a 24-well plate and treated with immuno-nanoparticles containing 20 μg/mL cdGMP, 17 μg/mL MPLA, or equivalent amounts of both cdGMP and MPLA. Cell culture supernatants were harvested 24 hr after seeding, clarified by centrifugation at 4°C, and analyzed per manufacturer's protocols for the presence of IFNα and IFNβ using LumiKine Xpress Bioluminescent cytokine ELISA kits from InvivoGen.

Immunostaining & confocal microscopy

4T1 tumor-bearing mice were injected with fluorescent nanoparticles and perfused 24 hr later with PBS and PBS containing 4% paraformaldehyde (Alfa Aesar, Haverhill, MA). Following euthanization, organs were harvested, fixed in 4% PFA/PBS, dehydrated in 30% sucrose/PBS, and embedded and frozen in OCT (Fisher Scientific, Hampton, NH). Primary (anti-CD31, anti-CD11c, anti-F4/80, anti-CD49b) and secondary antibodies were purchased from Thermo Fisher Scientific (Waltham, MA), Abcam (Cambridge, MA), and BioLegend (San Diego, CA). Frozen sections 10 μm in thickness were stained with 1:100–1:150 primary antibodies overnight at 4°C, followed by staining with 1:100–1:150 secondary antibodies for 1 hr at 25°C. Stained sections were mounted with No. 1.5 glass coverslips using Vectashield DAPI aqueous mounting medium (Vector Laboratories, Burlingame, CA) and imaged using a Leica TCS SP8 gated STED confocal microscope (Leica Microsystems, Buffalo Grove, IL).

Author Manuscript Author Manuscript Author Manuscript Author Manuscript

Transmission electron microscopy with negative staining

Carbon film grids were treated by glow discharge for 3 min. Liposomes were prepared in dilute suspensions (1:5–1:10 dilutions from treatment concentrations) and applied to treated grids and incubated for 30 s. Grids were washed 5x with 5 mM Tris buffer and directly afterwards stained 5x with 2% uranyl acetate. Imaging was performed using a Tecnai G2 SpiritBT electron microscope (FEI, Hillsboro, OR) operated at 80 kV.

Statistical Analysis

All statistical analyses are detailed in figure legends. Prism 7 (GraphPad Software) was used to analyze data by 1- or 2-way ANOVA with Tukey's or Sidak's post-test. *P* values less than 0.05 were considered statistically significant. Unless otherwise noted, all values are reported as the mean ± standard error of at least 3 independent biological replicates. In animal studies, at least 5 mice were included in each group.

RESULTS

Immuno-nanoparticles mediate the production of high levels of IFNβ, are stable *in vivo*, and drain with high efficiency to mammary tumors

To first define a quantitative rationale for our proposed systemic nanoparticle-mediated delivery platform, we investigated the mechanistic efficacy of delivering free immuno-agents both intravenously (i.v.) and intratumorally (i.t.) (Fig. 2). Importantly, while doses of up to 50 μg of free cdGMP administered i.t. are needed to regress early 4T1 primary tumors (27), to highlight a key advantage of nanoparticle encapsulation and systemic delivery, we elected to co-administer just 7 μg of free cdGMP and 6 μg of free MPLA i.v. or i.t., which are equivalent to doses that we aimed to deliver *via* immuno-NPs for therapeutic efficacy. Mice bearing orthotopic 4T1 primary tumors were treated with either free cdGMP and MPLA systemically (i.v.) or locally in the tumor (i.t.). Flow cytometry analysis 48 hr later indicated that there were no significant changes of major immune cell subsets in treated groups compared to controls in the blood (Fig. 2a), tumor (Fig. 2b), or spleen (Fig. 2c). In certain cases, immune cell populations decreased in treated mice compared to controls (i.e., blood neutrophils, tumor T and B cells, and splenic macrophages, $CD4^+$ T cells, and B cells). Notably, a reduction in tumor infiltrating T cells is directly correlated to advanced disease (39) and may be reflected in these free agonist treatments as early as 48 hr. These results strongly suggested that free cdGMP and MPLA delivered systemically or directly into the tumor had no therapeutic efficacy and clearly motivated the need for engineering a nanoparticle-mediated delivery strategy.

Towards this goal, we prepared ~60-nm liposomes containing equimolar quantities of DOPC and DPPC and 3 mol% mPEG2000-DSPE *via* ultrasonication. Transmission electron microscopy (TEM) was performed on negative-stained samples for analysis of lipid ultrastructure (Fig. 3a, white arrows indicate multilamellar nanoparticles). Dynamic light scattering (DLS) measurements indicated that nanoparticles were 61.2 ± 13.4 nm in diameter (Fig. 3b) and zeta potential measurements indicated a neutral surface charge (−5.4 ± 1.0 mV, Fig. 3c). Encapsulation efficiency of cdGMP was ~42% (Fig. 3d) and stability measurements indicated that hydrodynamic size remained the same over 24 hr (Fig. 3e).

Author Manuscript Author Manuscript Author Manuscript Author Manuscript

Release measurements of cdGMP at 37°C demonstrated that 14% of cdGMP was released after 3 hr and just 19% was released over 21 hr, suggesting that high cdGMP payloads could be stably delivered to tumor sites (Fig. 3f). To validate the function of these nanoparticles, we treated RAW 264.7 macrophages *in vitro* with equivalent amounts of nanoparticles containing cdGMP only, MPLA only, and both cdGMP and MPLA on the same particle (Fig. 3g). Cell culture supernatants were assayed for levels of secreted IFNα (Supplementary Fig. 1) and IFNβ (Fig. 3h) by ELISA after 24 hr. Both individual formulations mediated IFNβ production 19–25 times above background levels (Fig. 3h). Most significantly, however, immuno-NPs loaded with both cdGMP and MPLA induced a synergistic production of IFNβ that was 7–10 times the levels induced by nanoparticles carrying a single agonist alone (Fig. 3h). We therefore selected this co-loaded immuno-nanoparticle formulation for treatment studies *in vivo*.

We next quantified tumor homing efficiency of immuno-NPs. Mice bearing orthotopic 4T1 primary tumors were injected with fluorescent nanoparticles and live-animal Spectrum imaging was performed 24 hr later (Fig. 3i). Particle fluorescence appeared brightest per pixel basis in the region of the primary tumor and was predominantly co-localized with luminescence from luciferase-expressing tumor cells, suggesting that immuno-NPs drained with high efficiency to the primary tumor site (Fig. 3i). FMT imaging on excised tumors indicated that particle signal appeared to collect in distinct nodes (white and yellow arrows, Supplementary Fig. 2). To quantify tumor draining, 4T1 tumor-bearing mice were injected with fluorescent nanoparticles and perfused 4 hr and 28 hr later. Quantification of nanoparticle fluorescence obtained from Spectrum imaging indicated that 4.7% of immuno-NPs accumulated in tumor masses within 4 hr and this accumulation increased to 6.0% 28 hr post-injection (Fig. 3j). These data suggested that most of the tumor drainage occurred at a short time scale within hours after injection to the finite perivascular niche (Fig. 3j). Biodistribution analysis at 28 hr indicated that accumulation of immuno-NPs within the tumor compared to the liver, which is expected to have high retention due to its intrinsic clearance function, was similar per organ basis (Fig. 3k) and higher per gram tissue basis (Fig. 3l). Confocal microscopy analysis indicated that particles were found throughout the tissue from the tumor periphery to the center, often localizing in perivascular regions near the tumor vasculature as noted by CD31 staining for tumor endothelium (Supplementary Fig. 3a–b). Notably, nanoparticle signal often appeared punctate within individual cells, reminiscent of endosomal localization. Taken together, these data suggested that immuno-NPs are stable and drained with high efficiency to primary mammary tumors within 4 hr. Since safety considerations are paramount for systemically administered therapies, we injected healthy mice that did not bear tumors with immuno-NPs and assayed serum levels of alanine aminotransferase (ALT, Fig. 3m) and aspartate aminotransferase (AST, Fig. 3n) as a metric of hepatotoxicity. While AST levels were significantly elevated compared to untreated controls 1 day post-treatment, they dropped back to baseline within just 4 days. While mice injected with immuno-NPs lost ~10% of their weight within 24 hr, they regained this weight within 7 days with an additional ~8% weight gain within 3 weeks compared to controls (Fig. 3o). We highlight therefore that any immuno-NP-mediated toxicity is minimal and transient, with recovery observed within just 4–7 days.

Author Manuscript Author Manuscript Author Manuscript Author Manuscript

Immuno-nanoparticle treatment mediates upregulation of APCs and NK cells

We next performed flow cytometry analysis for the types of immune cells found both locally within the tumor as well as systemically in the blood and spleen 48 hr after treatment (Fig. 4). We used treatment with immune checkpoint inhibitors anti-programmed cell death protein-1 (anti-PD-1) and anti-cytotoxic T-lymphocyte-associated antigen-4 (anti-CTLA-4) as a metric of a clinically approved immunotherapy for comparison. Immuno-NP treatment very significantly increased DCs (11–13-fold), macrophages (5–10-fold), and NK cells (13–15-fold) in the blood compared to treatment with inhibitors and untreated controls (Fig. 4a). A representative dot plot for blood immune cells is shown in Fig. 4b. Similarly, immuno-NP treatment increased the number of DCs in the tumor 2.0-fold relative to untreated controls and also increased the numbers of tumor macrophages and NK cells 2.6–4.7-fold and 4.0–8.3-fold, respectively, compared to treatment with inhibitors and untreated controls (Fig. 4c). A representative dot plot for tumor immune cells is shown in Fig. 4d. Immuno-NPs also increased numbers of splenic macrophages 1.5–1.8-fold compared to mice treated with inhibitors and control mice (Fig. 4e). Fig. 4f shows a representative dot plot for splenic immune cells. The upregulation of APCs and NK cells in all three blood/tissue compartments suggested that immuno-NPs could mediate both an innate and adaptive immune response, which is important for long-term therapy. Notably, we also compared immune cell recruitment and activation with immuno-NPs that were actively targeted to unique molecules on the tumor-associated vasculature such as $\alpha_v\beta_3$ integrins and P-selectin (8,40) but these formulations did not have significant upregulation of immune cells compared to controls 48 hr post-treatment. We deduced from these early findings that targeted NPs are likely to be sequestered at target sites that may not be enriched in APCs, while untargeted NPs are free to drain to the perivascular areas for ready uptake by APCs.

Immuno-nanoparticle treatment drives reduction and control of primary tumor burden and prevents metastasis

To determine the efficacy of immuno-NPs in reducing primary tumor burden, we treated mice bearing advanced 4T1 mammary tumors twice intravenously with immuno-NPs, as noted (Fig. 5a–b, black arrows indicate treatment days). Within a day, tumor signal in mice treated with immuno-NPs decreased by 85% while tumor signal in both control groups increased by 55–57%. Tumors were excised post-treatment and mice treated with immuno-NPs had tumors that were a significant 50–60% reduced in mass compared to either control group (Fig. 5c, Supplementary Fig. 4). Notably, there were no statistical differences in tumor masses between control groups indicating that the vehicle alone had no effect in mediating treatment efficacy (Fig. 5c). We then treated mice bearing 4T1 orthotopic tumors with immuno-NPs either i.v. or i.t. alone or supplemented with anti-PD-1 and anti-CTLA-4. We compared these treatment groups to control groups where mice were given either free cdGMP and MPLA i.v. or i.t., inhibitors only, or left untreated (Supplemental Fig. 5a, black arrows indicate treatment days; weight monitoring data in Supplementary Fig. 5b). A week after the start of treatment, mice given free immune agonists i.v. had to be euthanized due to large and ulcerating primary tumors. We noted that in the untreated control group, smaller tumor cell bioluminescence signals especially during the latter stages of therapy (Supplementary Fig. 5a) did not correlate to smaller tumor sizes as measured by physical caliper measurements (Fig. 5d), indicating, as has been widely shown in the literature (15–

Author Manuscript Author Manuscript Author Manuscript Author Manuscript

17,19,22,24), that the 4T1 tumor mass is composed of a highly heterogeneous mixture of cells where non-tumor cells infiltrating the TME are often involved in advancing the cancer. From the start of treatment and up to one week afterwards, tumors of mice treated with immuno-NPs i.v. alone or with inhibitors significantly remained the smallest with volumes of ~170 mm^3 (data for day 5 post-treatment in Fig. 5d).

To establish a mechanistic framework for immuno-NP uptake and function within the primary tumor, we next treated 4T1 tumor-bearing mice with two consecutive daily doses of fluorescent immuno-NPs and analyzed for cellular uptake by flow cytometry. Compared to mice injected with empty NPs, mice treated with immuno-NPs had significantly elevated numbers of $CD45^+$ immune cells and NK cells per gram of tumor tissue (Fig. 5e). Further, there was a significantly increased number of cells that had taken up NPs in these treated mice, while levels of uptake within tumor cells, $CD45^+$ immune cells, DCs, macrophages, and NK cells were statistically similar (Fig. 5f). Notably, while ~53% of NPs were taken up by $CD45^+$ immune cells (~3% by DCs, ~9% by macrophages, and ~33% by NK cells), only ~0.9% of NPs were taken up by tumor cells, indicating that perivascular accumulation was optimal for targeting of APCs and NK cells *in lieu* of tumor cells, since this niche is enriched for these immune cells (Fig. 5f). Further analysis also demonstrated that DCs in particular endocytosed significantly more immuno-NPs within the primary tumor (Fig. 5g), and that these NP^+ DCs produced significantly more IFNβ (Fig. 5h). To investigate longer-term efficacy, blood and tumors were harvested from these mice 7 and 14 days post-treatment and assayed for immune cell content by flow cytometry. Compared to untreated controls, DCs were significantly elevated in the blood 7 days post-treatment (Fig. 5i), with no statistical differences in $CD4^+$ T cells (Fig. 5j). Notably, $CD8^+$ T cells were significantly elevated in the blood 14 days post-treatment (Fig. 5k). Intratumoral DCs (Fig. 5l) and NK cells (Fig. 5m) were similarly elevated per gram of tumor tissue 7 days post-treatment, with no statistical differences in numbers of intratumoral T cells (Fig. 5n–o).

To determine the efficacy of immuno-NPs in treating metastasis, we treated 4T1 tumor-bearing mice with immuno-NPs with and without checkpoint inhibitors i.v. or i.t. and free agonists i.v. or i.t. (Fig. 6a, black arrows indicate treatment days). From all the formulations, it was only immuno-NPs administered i.v. that completely prevented metastasis in the lungs and lymph nodes (Fig. 6a). Twelve days after the start of treatment, metastatic signal in mice treated with immuno-NPs i.v. remained near baseline and significantly lower than signal in mice treated with free agonists i.t., immuno-NPs i.t. with inhibitors, and inhibitors only (Fig. 6a; representative bioluminescence images of metastasis shown in Fig. 6b). Notably 12 days post-treatment, while none of the mice treated with immuno-NPs i.v. had a metastatic signal above threshold (dashed grey line in Fig. 6a), 50–100% of mice in all other groups had increased signal. As with the primary tumor, we then sought to establish a mechanistic framework for immuno-NP uptake and function within lungs that contained metastases. To this end, we treated 4T1 tumor-bearing mice with two consecutive daily doses of fluorescent immuno-NPs and analyzed for cellular uptake by flow cytometry. Compared to mice injected with empty NPs, mice treated with immuno-NPs had significantly elevated numbers of $CD45^+$ immune cells, macrophages, and NK cells per gram of lung tissue (Fig. 6c). There were significantly more cells in treated mice that had taken up NPs (Fig 6d) and while ~53% of these NP^+ cells were $CD45^+$ immune cells (and significantly so), only ~0.2% of cells that

Author Manuscript Author Manuscript Author Manuscript Author Manuscript

had taken up NPs in the lungs were tumor cells (Fig. 6d). Representative flow cytometry dot plots for NP^+ cells are shown in Fig. 6e. Strikingly, in mice that were treated with immuno-NPs, lung DCs and macrophages had endocytosed significantly more NPs (Fig. 6f) and these NP^+ DCs and macrophages produced significantly more IFNβ (Fig. 6g). Confocal microscopy studies indicated that immuno-NPs were found largely in the vicinity of tumor cells in the lungs and in close proximity to DCs (Fig. 6h), macrophages (Fig. 6i), and NK cells (Fig. 6j), indicating that this immune response was tumor-associated and not non-specific. In areas of the lungs that did not contain metastases, immuno-NPs were also largely absent (Supplementary Fig. 6).

Finally, to establish the broader impact of the efficacy of this immuno-NP treatment to other aggressive cancers, we investigated their therapeutic efficacy in the treatment of mice bearing orthotopic B16F10 melanoma tumors (Fig. 7). We treated tumor-bearing mice with two consecutive daily doses of immuno-NPs and observed that tumor volume dropped by 50% in treated mice compared to controls within a single day and continued to remain a significant 50–65% reduced over the course of 2 weeks (Fig. 7a, black arrows indicated treatment days). Survival in treated mice was also significantly increased compared to controls (Fig. 7b; weight monitoring data in Supplementary Fig. 7). Blood flow cytometry analysis indicated significantly elevated levels of DCs (Fig. 7c). There were no statistical differences in levels of blood NK cells (Fig. 7d) and $CD4^+$ T cells (Fig. 7e). Importantly, $CD8^+$ T cells was significantly elevated in blood even 7 days post-treatment and continued to increase 14 days post-therapy (Fig. 7f). Taken together, these results indicate that the therapeutic efficacy of immuno-NPs can be translated across multiple models of aggressive cancer.

DISCUSSION

While immune agonists can generate powerful anti-tumor immunity, their successful delivery to the TME relies on efficiently accessing the tumor microvasculature, minimizing off-target toxicity, and, in the case of multiple synergistic therapeutics, targeting the same cell (6–10,12,14). Here, we elected to co-encapsulate STING agonist cdGMP (27,29–32) and TLR4 agonist MPLA (28,34) within a single liposomal nanoparticle and exploited systemic delivery to access the leaky tumor microvasculature in entirety. Our delivery strategy mediated preferential collection within the perivascular areas of the TME that are rich in APCs. Co-encapsulation within a nanoparticle not only prevents cdGMP/MPLA-induced off-target systemic toxicity, but also guarantees delivery to the same target APCs. The success of this large class of immunotherapies relies on these absolute fundamental advantages of nanoparticle-mediated systemic delivery. In the case of the primary tumor, systemic delivery enables immuno-NP accumulation within the APC-rich perivascular areas of the tumor, which may drive preferential accumulation of immuno-NPs within $CD45^+$ immune cells compared to tumor cells. DCs, macrophages, and NK cells are highly efficient phagocytes compared to tumor cells that are also notoriously poor antigen presenters. In the case of metastasis, it can be argued that systemic delivery may be the singular route of efficient access. Given that both cdGMP and MPLA are strong inducers of Type I interferons and share common downstream effectors such as NF-κB and IRF3 (41,42), the IFNβ synergy we measured as a result of co-encapsulation of both agonists is likely due to

Author Manuscript Author Manuscript Author Manuscript Author Manuscript

amplification of these downstream pathways. IFNβ drives robust innate immunity, NK cell activity, and APC-mediated activation of $CD8^+$ T cells (2,24). It is also pivotal in preventing malignant transformation and de-differentiating cancer stem cells (43–45).

Our mechanistic analysis has demonstrated that treatment efficacy depends on the accumulation of immuno-NPs at the site of the primary tumor or metastases, their uptake by local APCs, and the production of IFNβ by these cells. Notably, we have shown these APCs endocytose a significantly greater number of immuno-NPs. We also observed significantly increased levels of blood $CD8^+$ T cells in mice treated with immuno-NPs, indicating a functioning vaccination mechanism, where activated tumor-resident DCs can travel to lymph nodes to prime systemic T cells and mediate their recruitment back to the site of the tumor. These data further demonstrate that NK cells are a significant contributor to efficacy, and their role is highly advantageous since they are not only direct-killing initial responders but can also be involved in the formation of memory NK cells.

CONCLUSIONS

In conclusion, we have constructed a versatile lipid-based immuno-NP platform that serves to mount a robust anti-tumor immune response by accumulating with high efficiency in the APC-rich perivascular regions of primary tumors and metastases and inducing the strong production of IFNβ. We have shown that synergy between cdGMP and MPLA co-encapsulated in the same nanoparticle drives the production of high levels of IFNβ and mediates a robust APC- and NK cell-driven anti-tumor immune response. Finally, we have shown that immuno-particles delivered systemically *via* the vasculature outperform even intratumoral delivery and serve to reduce and limit the growth of the primary tumor and prevent metastasis without the need for additional supplementation with clinically approved checkpoint inhibitors. This nanotechnology platform serves to effectively reverse significant TME immunosuppression and this approach shows much promise for nanoparticle platforms that similarly aim to ‘re-engineer’ TME immunity.

Supplementary Material

Refer to Web version on PubMed Central for supplementary material.

Acknowledgements

This work was supported by grants from the National Cancer Institute (R01CA177716, U01CA198892), the Alex’s Lemonade Stand Foundation, and the Angie Fowler AYA Cancer Research Initiative of the Case Comprehensive Cancer Center (E.K.). P.A.B. was supported by a graduate research fellowship from NSF. G.C. was supported by a fellowship from the NIH Interdisciplinary Biomedical Imaging Training Program (T32EB007509) administered by the Department of Biomedical Engineering, Case Western Reserve University. We acknowledge the Case Center for Imaging Research, Case Comprehensive Cancer Center Flow Cytometry Core, and the Case School of Medicine Light Microscopy Core Facility and support from NIH S10-RR031845. We further acknowledge Mei Yin and the Cleveland Clinic Lerner Research Institute Imaging Core for assistance with negative staining and electron microscopy. We also thank the University Hospitals Pathology Core for assistance with ALT/AST measurements.

REFERENCES

1. Joyce JA, Fearon DT. T cell exclusion, immune privilege, and the tumor microenvironment. Science 2015;348:74–80 [PubMed: 25838376]

Author Manuscript Author Manuscript Author Manuscript Author Manuscript

2. Muller L, Aigner P, Stoiber D. Type I Interferons and Natural Killer Cell Regulation in Cancer. Frontiers in immunology 2017;8:304 [PubMed: 28408907]

3. Swartz MA, Hirosue S, Hubbell JA. Engineering approaches to immunotherapy. Science translational medicine 2012;4:148rv9

4. Larkin J, Chiarion-Sileni V, Gonzalez R, Grob JJ, Cowey CL, Lao CD, et al. Combined Nivolumab and Ipilimumab or Monotherapy in Untreated Melanoma. The New England journal of medicine 2015;373:23–34 [PubMed: 26027431]

5. Linch SN, Kasiewicz MJ, McNamara MJ, Hilgart-Martiszus IF, Farhad M, Redmond WL. Combination OX40 agonism/CTLA-4 blockade with HER2 vaccination reverses T-cell anergy and promotes survival in tumor-bearing mice. Proceedings of the National Academy of Sciences of the United States of America 2016;113:E319–27 [PubMed: 26729864]

6. Moynihan KD, Opel CF, Szeto GL, Tzeng A, Zhu EF, Engreitz JM, et al. Eradication of large established tumors in mice by combination immunotherapy that engages innate and adaptive immune responses. Nature medicine 2016;22:1402–10

7. Zhang Y, Li N, Suh H, Irvine DJ. Nanoparticle anchoring targets immune agonists to tumors enabling anti-cancer immunity without systemic toxicity. Nature communications 2018;9:6

8. Atukorale PU, Covarrubias G, Bauer L, Karathanasis E. Vascular targeting of nanoparticles for molecular imaging of diseased endothelium. Adv Drug Deliv Rev 2017;113:141–56 [PubMed: 27639317]

9. Decuzzi P, Ferrari M. Design maps for nanoparticles targeting the diseased microvasculature. Biomaterials 2008;29:377–84 [PubMed: 17936897]

10. Murphy EA, Majeti BK, Barnes LA, Makale M, Weis SM, Lutu-Fuga K, et al. Nanoparticle-mediated drug delivery to tumor vasculature suppresses metastasis. Proceedings of the National Academy of Sciences of the United States of America 2008;105:9343–8 [PubMed: 18607000]

11. Andre F, Zielinski CC. Optimal strategies for the treatment of metastatic triple-negative breast cancer with currently approved agents. Ann Oncol 2012;23 Suppl 6:vi46–51 [PubMed: 23012302]

12. Atkins M Immunotherapy Combinations With Checkpoint Inhibitors in Metastatic Melanoma: Current Approaches and Future Directions. Seminars in oncology 2015;42 Suppl 3:S12–9 [PubMed: 26598055]

13. Michallet M, Maloisel F, Delain M, Hellmann A, Rosas A, Silver RT, et al. Pegylated recombinant interferon alpha-2b vs recombinant interferon alpha-2b for the initial treatment of chronic-phase chronic myelogenous leukemia: a phase III study. Leukemia 2004;18:309–15 [PubMed: 14671645]

14. Hubbell JA, Thomas SN, Swartz MA. Materials engineering for immunomodulation. Nature 2009;462:449–60 [PubMed: 19940915]

15. Dent R, Trudeau M, Pritchard KI, Hanna WM, Kahn HK, Sawka CA, et al. Triple-negative breast cancer: clinical features and patterns of recurrence. Clinical cancer research : an official journal of the American Association for Cancer Research 2007;13:4429–34

16. Haffty BG, Yang Q, Reiss M, Kearney T, Higgins SA, Weidhaas J, et al. Locoregional relapse and distant metastasis in conservatively managed triple negative early-stage breast cancer. Journal of clinical oncology : official journal of the American Society of Clinical Oncology 2006;24:5652–7 [PubMed: 17116942]

17. Pulaski BA, Ostrand-Rosenberg S. Mouse 4T1 breast tumor model. Curr Protoc Immunol 2001;Chapter 20:Unit 20 2

18. Bertucci F, Finetti P, Birnbaum D. Basal breast cancer: a complex and deadly molecular subtype. Curr Mol Med 2012;12:96–110 [PubMed: 22082486]

19. Bertucci F, Finetti P, Cervera N, Charafe-Jauffret E, Buttarelli M, Jacquemier J, et al. How different are luminal A and basal breast cancers? Int J Cancer 2009;124:1338–48 [PubMed: 19058218]

20. Cancer Genome Atlas N Comprehensive molecular portraits of human breast tumours. Nature 2012;490:61–70 [PubMed: 23000897]

21. Coghlin C, Murray GI. Current and emerging concepts in tumour metastasis. J Pathol 2010;222:1–15 [PubMed: 20681009]

22. Perou CM, Sorlie T, Eisen MB, van de Rijn M, Jeffrey SS, Rees CA, et al. Molecular portraits of human breast tumours. Nature 2000;406:747–52 [PubMed: 10963602]

Author Manuscript Author Manuscript Author Manuscript Author Manuscript

23. Perreard L, Fan C, Quackenbush JF, Mullins M, Gauthier NP, Nelson E, et al. Classification and risk stratification of invasive breast carcinomas using a real-time quantitative RT-PCR assay. Breast Cancer Res 2006;8:R23 [PubMed: 16626501]
24. van Zijl F, Krupitza G, Mikulits W. Initial steps of metastasis: cell invasion and endothelial transmigration. Mutat Res 2011;728:23–34 [PubMed: 21605699]
25. Hanahan D, Weinberg RA. Hallmarks of cancer: the next generation. Cell 2011;144:646–74 [PubMed: 21376230]
26. Miller MA, Zheng YR, Gadde S, Pfirschke C, Zope H, Engblom C, et al. Tumour-associated macrophages act as a slow-release reservoir of nano-therapeutic Pt(IV) pro-drug. Nature communications 2015;6:8692
27. Corrales L, Glickman LH, McWhirter SM, Kanne DB, Sivick KE, Katibah GE, et al. Direct Activation of STING in the Tumor Microenvironment Leads to Potent and Systemic Tumor Regression and Immunity. Cell reports 2015;11:1018–30 [PubMed: 25959818]
28. Mata-Haro V, Cekic C, Martin M, Chilton PM, Casella CR, Mitchell TC. The vaccine adjuvant monophosphoryl lipid A as a TRIF-biased agonist of TLR4. Science 2007;316:1628–32 [PubMed: 17569868]
29. Corrales L, Gajewski TF. Molecular Pathways: Targeting the Stimulator of Interferon Genes (STING) in the Immunotherapy of Cancer. Clinical cancer research : an official journal of the American Association for Cancer Research 2015;21:4774–9 [PubMed: 26373573]
30. Corrales L, Gajewski TF. Endogenous and pharmacologic targeting of the STING pathway in cancer immunotherapy. Cytokine 2016;77:245–7 [PubMed: 26315534]
31. Corrales L, McWhirter SM, Dubensky TW Jr., Gajewski TF. The host STING pathway at the interface of cancer and immunity. The Journal of clinical investigation 2016;126:2404–11 [PubMed: 27367184]
32. Woo SR, Fuertes MB, Corrales L, Spranger S, Furdyna MJ, Leung MY, et al. STING-dependent cytosolic DNA sensing mediates innate immune recognition of immunogenic tumors. Immunity 2014;41:830–42 [PubMed: 25517615]
33. Nakamura T, Miyabe H, Hyodo M, Sato Y, Hayakawa Y, Harashima H. Liposomes loaded with a STING pathway ligand, cyclic di-GMP, enhance cancer immunotherapy against metastatic melanoma. Journal of controlled release : official journal of the Controlled Release Society 2015;216:149–57 [PubMed: 26282097]
34. Pouliot K, Buglione-Corbett R, Marty-Roix R, Montminy-Paquette S, West K, Wang S, et al. Contribution of TLR4 and MyD88 for adjuvant monophosphoryl lipid A (MPLA) activity in a DNA prime-protein boost HIV-1 vaccine. Vaccine 2014;32:5049–56 [PubMed: 25045815]
35. Koshy STC, A. S, Gu L, Graveline AR, Mooney DJ Liposomal Delivery Enhances Immune Activation by STING Agonists for Cancer Immunotherapy. Advanced BioSystems 2017;1
36. Hanson MC, Crespo MP, Abraham W, Moynihan KD, Szeto GL, Chen SH, et al. Nanoparticulate STING agonists are potent lymph node-targeted vaccine adjuvants. The Journal of clinical investigation 2015;125:2532–46 [PubMed: 25938786]
37. Fang J, Nakamura H, Maeda H. The EPR effect: Unique features of tumor blood vessels for drug delivery, factors involved, and limitations and augmentation of the effect. Advanced drug delivery reviews 2011;63:136–51 [PubMed: 20441782]
38. Maruyama K Intracellular targeting delivery of liposomal drugs to solid tumors based on EPR effects. Advanced drug delivery reviews 2011;63:161–9 [PubMed: 20869415]
39. Koch M, Beckhove P, Op den Winkel J, Autenrieth D, Wagner P, Nummer D, et al. Tumor infiltrating T lymphocytes in colorectal cancer: Tumor-selective activation and cytotoxic activity in situ. Annals of surgery 2006;244:986–92; discussion 92–3 [PubMed: 17122624]
40. Ruoslahti E Specialization of tumour vasculature. Nature reviews Cancer 2002;2:83–90 [PubMed: 12635171]
41. Chen Q, Sun L, Chen ZJ. Regulation and function of the cGAS-STING pathway of cytosolic DNA sensing. Nature immunology 2016;17:1142–9 [PubMed: 27648547]
42. Luan L, Patil NK, Guo Y, Hernandez A, Bohannon JK, Fensterheim BA, et al. Comparative Transcriptome Profiles of Human Blood in Response to the Toll-like Receptor 4 Ligands

Author Manuscript Author Manuscript Author Manuscript Author Manuscript

Lipopolysaccharide and Monophosphoryl Lipid A. Scientific reports 2017;7:40050 [PubMed: 28053314]

43. Dalerba P, Cho RW, Clarke MF. Cancer stem cells: models and concepts. Annu Rev Med 2007;58:267–84 [PubMed: 17002552]
44. Mani SA, Guo W, Liao MJ, Eaton EN, Ayyanan A, Zhou AY, et al. The epithelial-mesenchymal transition generates cells with properties of stem cells. Cell 2008;133:704–15 [PubMed: 18485877]
45. Santisteban M, Reiman JM, Asiedu MK, Behrens MD, Nassar A, Kalli KR, et al. Immune-induced epithelial to mesenchymal transition in vivo generates breast cancer stem cells. Cancer research 2009;69:2887–95 [PubMed: 19276366]

Author Manuscript Author Manuscript Author Manuscript Author Manuscript

Statement of Significance

Systemic administration of an immuno-nanoparticle in a murine breast tumor model drives a robust tumor site-specific antigen-presenting cell response by delivering two synergistic immune-potentiating molecules, highlighting the potential of nanoparticles for immunotherapy.

Author Manuscript Author Manuscript Author Manuscript Author Manuscript

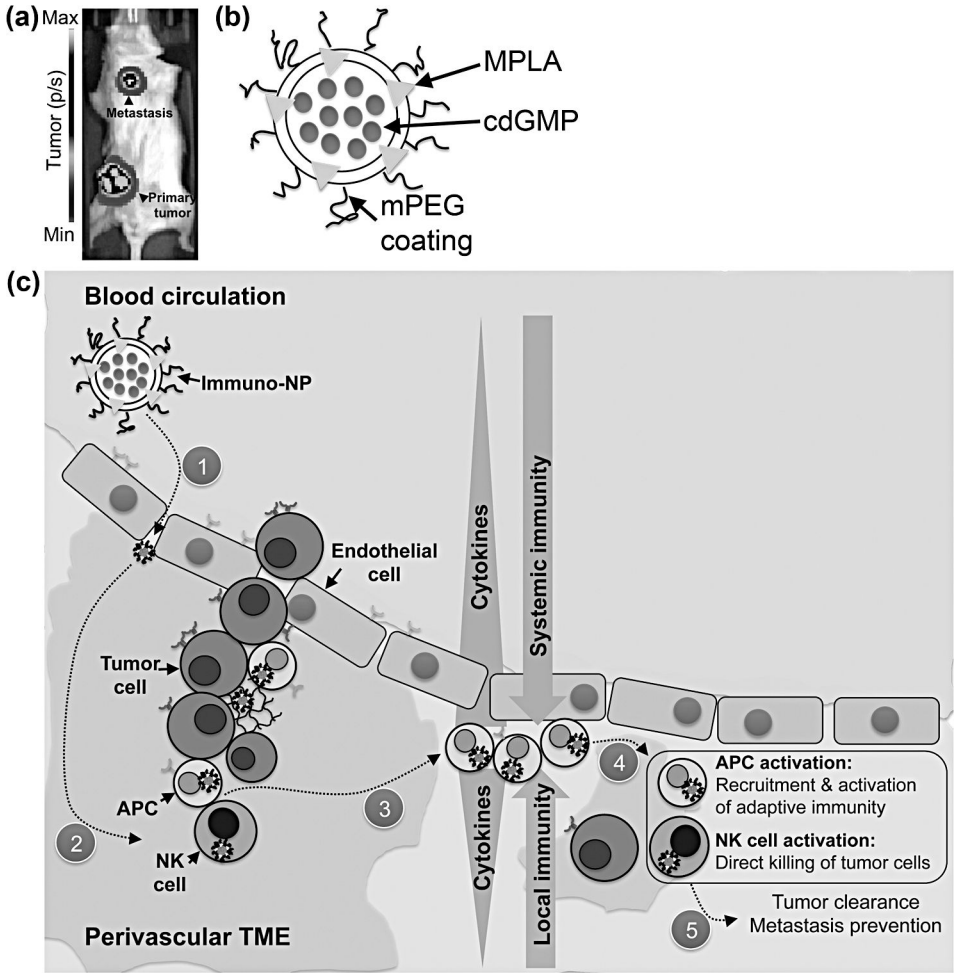

Figure 1.

Schematic of nanoparticle/treatment platform. **(a)** Representative image of 4T1 tumor-bearing mouse with both an orthotopic primary tumor mass and lung metastasis (tumor cells express luciferase and luminescence units are photons/s). **(b)** Schematic of a ~60-nm immuno-NP with surface mPEG and encapsulating both hydrophilic cdGMP within the core (blue) and hydrophobic MPLA within the lipid bilayer (red). **(c)** Schematic of treatment platform where immuno-NPs are delivered systemically to home to tumor sites and collect within the tumor microenvironment (1). Internalization of immuno-NPs (2) results in a tumor site-specific cytokine gradient (3) that in turn leads to APC- and NK cell-driven recruitment and activation of both local and systemic immune cells (4) that mount a robust attack to mediate tumor clearance (5).

Author Manuscript Author Manuscript Author Manuscript Author Manuscript

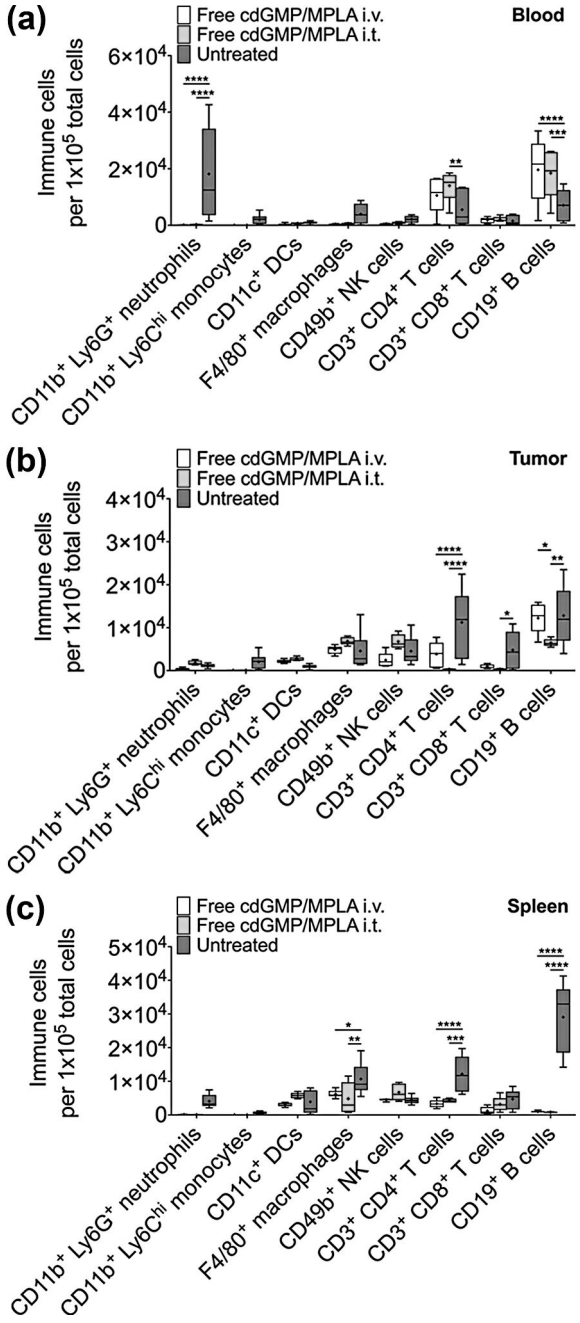

Figure 2.

Treatment with free cdGMP and MPLA i.v. or i.t. does not elicit a sufficient immune response. Flow cytometry analysis of immune cells in the blood **(a)**, tumor **(b)**, and spleen **(c)** of 4T1 orthotopic mammary tumor-bearing mice 48 hr after treatment with 7 μg cdGMP and 6 μg MPLA i.v. or i.t. Treatment groups were made up of 5–6 mice (the untreated group contained 10–15 mice), data are plotted as box and whiskers plots (5–95 percentile, + designates the mean) with statistics by 2-way ANOVA with Tukey's post-test (* $P<0.05$, ** $P<0.01$, *** $P<0.001$, **** $P<0.0001$).

Author Manuscript Author Manuscript Author Manuscript Author Manuscript

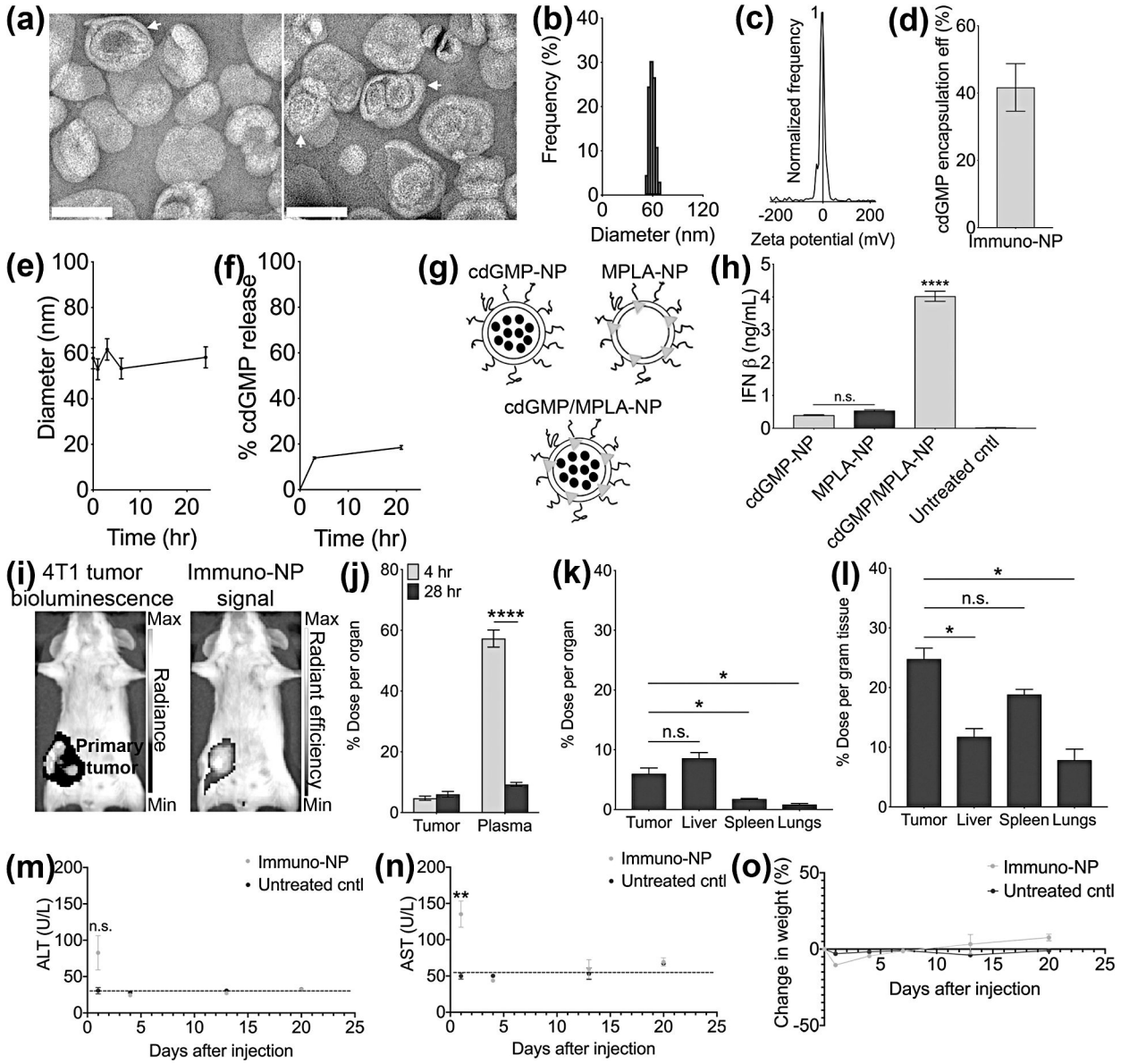

Figure 3.

Immuno-NPs are stable and function effectively to synergistically harness multiple innate immune pathways. Negative-stained TEM of immuno-liposomes (scale bars are 100 nm, white arrows note multilamellar nanoparticles) **(a)**. DLS analysis for immuno-nanoparticle size **(b)** and zeta potential **(c)**. Immuno-nanoparticle cdGMP encapsulation efficiency **(d)** and stability in terms of hydrodynamic size by DLS **(e)** and cdGMP release **(f)**. Cartoon schematics of nanoparticle formulations used for ELISA analysis **(g)** for *in vitro* production of IFNβ **(h)**. **(i)** Live-animal Spectrum imaging for tumor cell bioluminescence (left panel, units of radiance is photons/second) and DiD-labeled nanoparticle fluorescence (right panel, units of radiant efficiency are [photons/s]/[μW/cm^2]) 24 hr after i.v. injection. Quantification of targeting from *ex vivo* organs and plasma of mice injected with fluorescent DiD-nanoparticles plotted as % dose per organ **(j)** at 4- and 28 hr post-injection i.v.. Biodistribution at 28 hr is plotted as mean ± standard error of % dose per organ (**k**) and %

Author Manuscript Author Manuscript Author Manuscript Author Manuscript

dose per gram tissue (**l**). ALT **(m)** and AST **(n)** measurements in enzyme units/L (dashed lines indicate average baseline levels of healthy mice) with corresponding mouse weight measurements **(o)** for N=5 mice per group. All conditions were performed at least in triplicate and plotted as mean ± standard error with statistics by 1-/2-way ANOVA with Tukey's/Sidak's post-test (* P<0.05, ** P<0.01, **** P<0.0001). DLS data are plotted as mean ± standard deviation.

Author Manuscript Author Manuscript Author Manuscript Author Manuscript

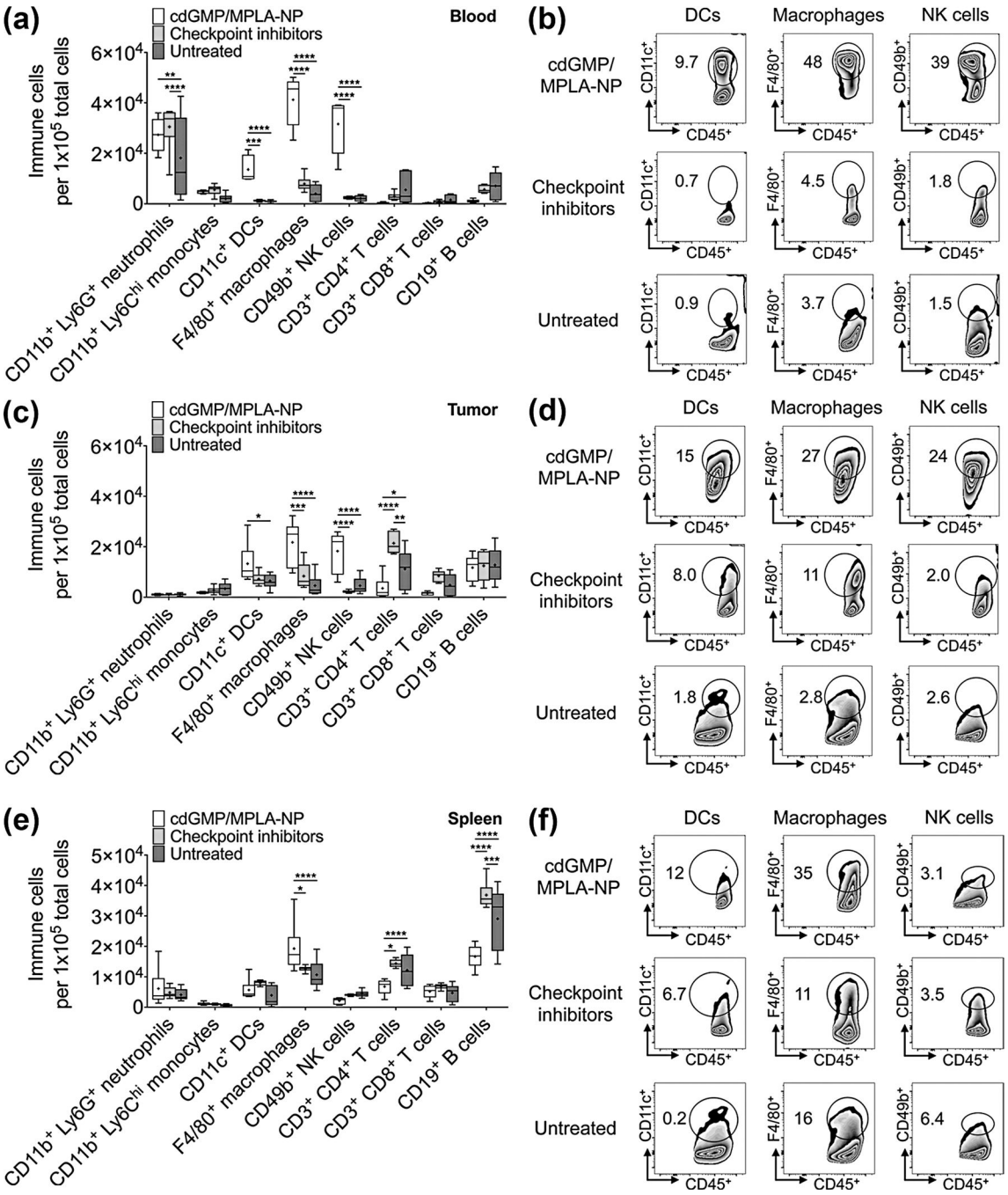

Figure 4.

Treatment with immuno-NPs elicits a robust APC- and NK cell-driven immune response. Flow cytometry analysis of immune cells in the blood **(a)**, tumor **(c)**, and spleen **(e)** of 4T1 orthotopic mammary tumor-bearing mice 48 hr after treatment with immuno-nanoparticles (carrying 7 μg cdGMP and 6 μg MPLA) i.v. or immune checkpoint inhibitors (250 μg anti-PD1 and 100 μg anti-CTLA4 i.v.). Representative flow cytometry dot plots for significant immune cell subtypes are shown for each tissue type blood **(b)**, tumor **(d)**, and spleen **(f)**. Treatment groups were made up of 6 mice, data are plotted as box and whiskers plots (5–95

Author Manuscript Author Manuscript Author Manuscript Author Manuscript

percentile, + designates the mean) with statistics by 2-way ANOVA with Tukey's post-test (* P<0.05, ** P<0.01, *** P<0.001, **** P<0.0001).

Author Manuscript Author Manuscript Author Manuscript Author Manuscript

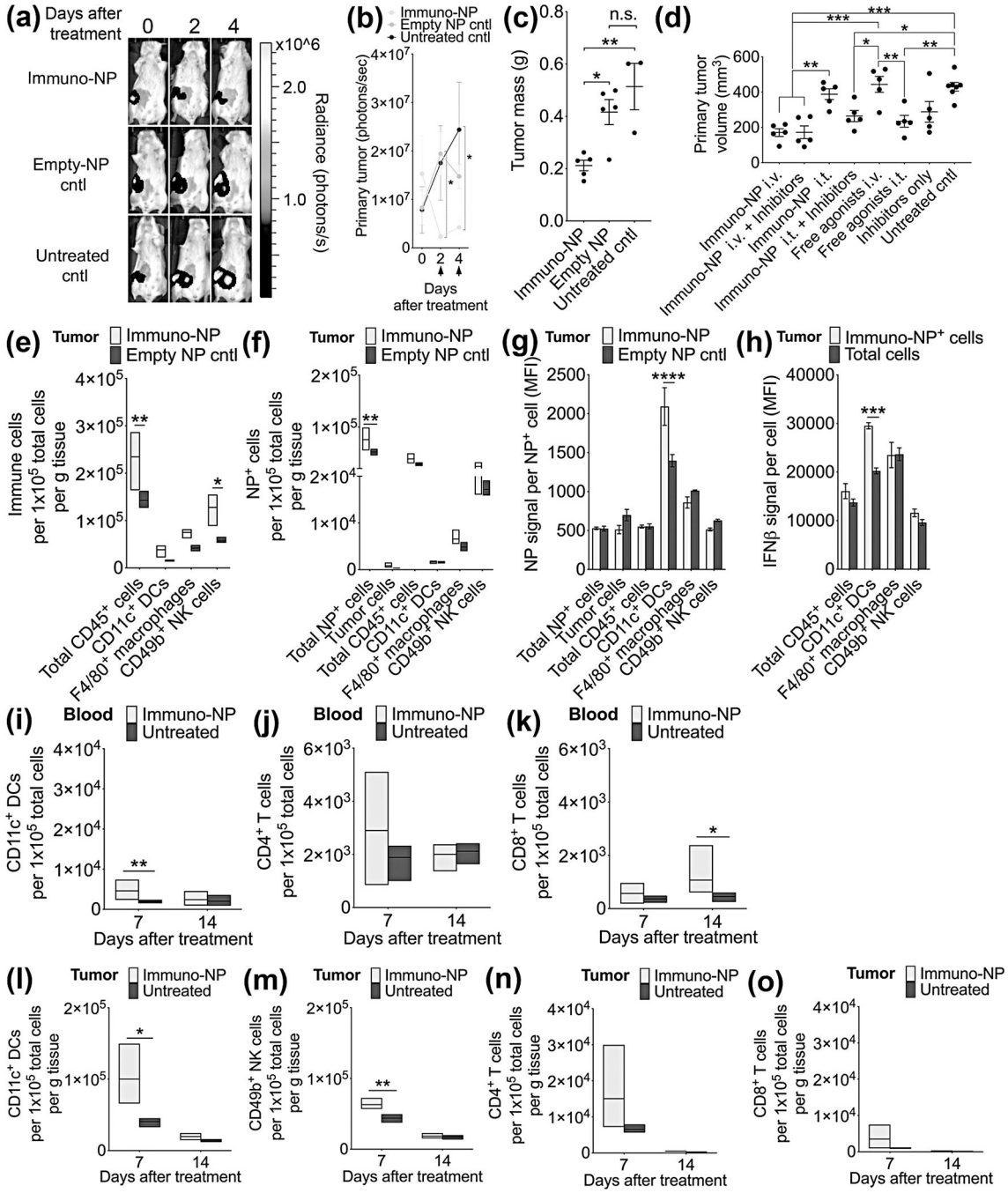

Figure 5.

Immuno-NP treatment results in a substantial reduction in primary tumor mass with DC and NK cell effectors in the 4T1 model. **(a)** Representative bioluminescence images of 4T1 tumor-bearing mice from 3 treatment groups (immuno-NPs, empty NPs as vehicle control, and untreated controls) treated twice 2 days apart with tumors removed surgically 4 days after the start of treatment. Units of radiance are photons/s. Black arrows along x-axis designate treatment days. **(b)** Quantification of primary tumor cell luminescence as treatment was monitored. Nanoparticle groups had 5 mice per group while untreated control

Author Manuscript Author Manuscript Author Manuscript Author Manuscript

group had 3 mice. **(c)** Quantification of masses of excised tumors 4 days after the start of treatment. **(d)** Primary tumor volume measurements on day 5 after the start of treatment (N=5 mice per group). Flow cytometry analysis of immune cells per gram of tumor tissue **(e)**, NP^+ cells **(f)**, NP signal per NP^+ cell **(g)**, and IFNβ per cell **(h)** (N=4 mice per group). Flow cytometry analysis of blood DCs **(i)**, $CD4^+$ T cells **(j)**, and $CD8^+$ T cells **(k)**, and tumor DCs **(l)**, NK cells **(m)**, $CD4^+$ T cells **(n)**, and $CD8^+$ T cells **(o)** (N=4 mice per group). Mean ± standard error are plotted with statistics by 1-/2-way ANOVA with Tukey's post-test (* $P<0.05$, ** $P<0.01$, *** $P<0.001$).

Author Manuscript Author Manuscript Author Manuscript Author Manuscript

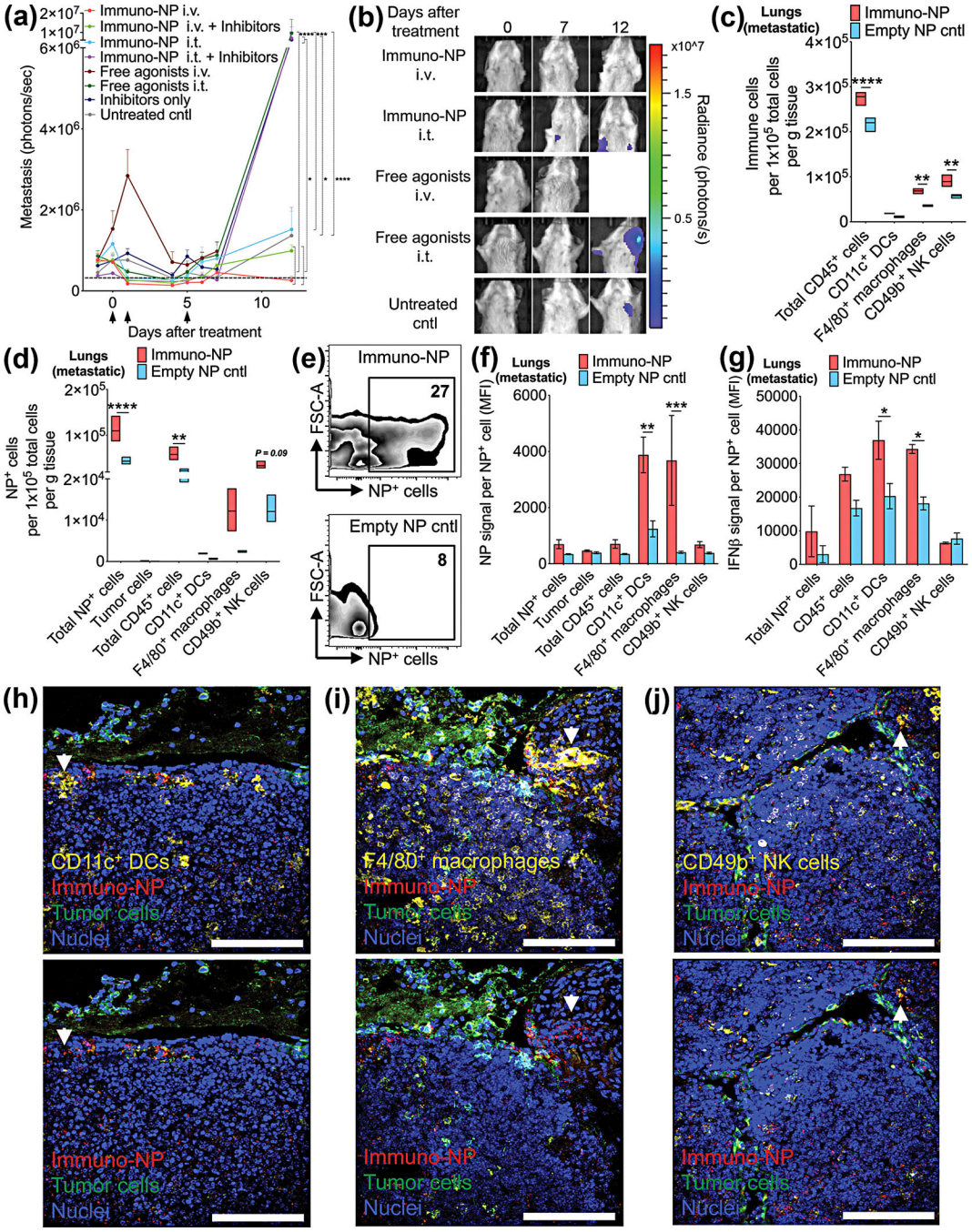

Figure 6.

Immuno-NPs mediate the prevention of metastasis in the 4T1 model. **(a)** Bioluminescence quantification of lung/lymph node metastasis signal for each treatment group (N=5–7 mice per group). Black arrows along x-axis designate treatment days. **(h)** Representative bioluminescence images of metastasis. Units of radiance are photons/s. Flow cytometry analysis of immune cells per gram of tumor tissue **(c)**, NP^+ cells **(d)**, representative dot plots **(e)**, NP signal per NP^+ cell **(f)**, and IFNβ per cell **(g)** (N=4 mice per group). Mean ± standard error are plotted with statistics by 1-/2-way ANOVA with Tukey's post-test (*

Author Manuscript Author Manuscript Author Manuscript Author Manuscript

P<0.05, ** P<0.01, *** P<0.001, *** P<0.0001). Confocal microscopy of metastatic lung tissue sections with staining for DCs **(h)**, macrophages **(i)**, and NK cells **(j)**. White arrows indicate areas with immuno-NPs. Scale bars are 100 μm.

Author Manuscript Author Manuscript Author Manuscript Author Manuscript

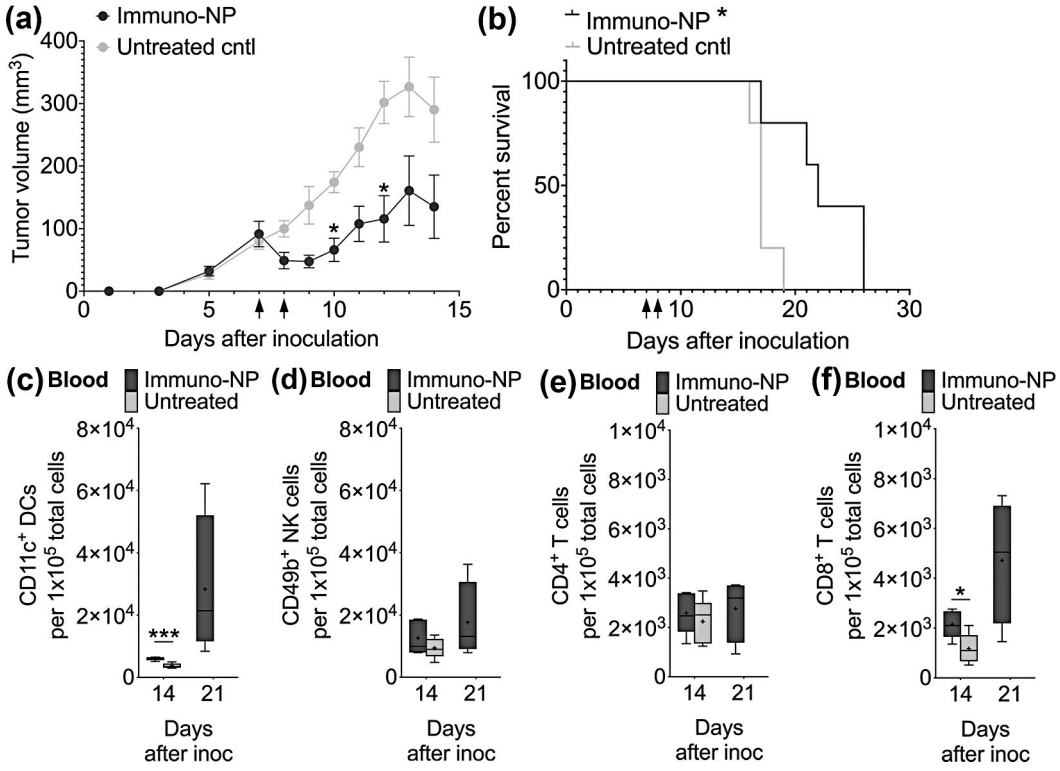

Figure 7.

Immuno-NP treatment has significant efficacy in the treatment of B16F10 melanoma. **(a)** Tumor volume measurements, where black arrows on x-axis designate treatment days (N=5 mice per group). **(b)** Kaplan-Meier survival analysis. Flow cytometry analysis for blood DCs **(c)**, NK cells **(d)**, $CD4^+$ T cells **(e)**, and $CD8^+$ T cells **(f)**. Mean ± standard error are plotted with statistics by 1-/2-way ANOVA with Tukey's post-test (* $P<0.05$, *** $P<0.001$).